Acta Crystallographica Section D
Biological Crystallography
ISSN 0907-4449

Crystal structure of δ-chymotrypsin bound to a peptidyl chloromethyl ketone inhibitor

Aengus Mac Sweeney,[a]*† Gabriel Birrane,[a] Martin A. Walsh,[b]‡ Timothy O'Connell,[c]§ J. Paul G. Malthouse[c] and Timothy M. Higgins[a]

[a]Department of Chemistry, NUI Galway, Galway, Ireland, [b]European Molecular Biology Laboratory (EMBL), c/o DESY, Notkestrasse 85, D-22603 Hamburg, Germany, and [c]Department of Biochemistry, University College, Dublin, Ireland

† Present address: Universität Zürich, Biochemisches Institüt, Winterthurer Strasse 190, CH-8057 Zürich, Switzerland.
‡ Present address: IRBM 'P. Angeletti', Via Pontina KM 30.600, 00040 Pomezia (Rome), Italy.
§ Present address: Max-Planck-Institut für Züchtungsforschung, Carl-von-Linné-Weg 10, D-50829 Koln, Germany.

Correspondence e-mail: macsweeney@biocfebs.unizh.ch

Received 17 August 1999
Accepted 20 December 1999

PDB Reference: δ-chymotrypsin complex, 1dlk.

Chymotrypsin is a member of the trypsin family of serine proteases and is one of the first proteins successfully studied by X-ray crystallography. It is secreted into the intestine as the inactive precursor chymotrypsinogen; four sequential cleavages of the peptide bonds following residues 13, 15, 146 and 148 occur to generate the active π, δ, κ and α forms of chymotrypsin. ^{13}C NMR has shown [O'Connell & Malthouse (1995). *Biochem. J.* **307**, 353–359] that when the δ form of chymotrypsin is inhibited by 2-^{13}C-enriched benzyloxycarbonylglycylglycylphenylalanyl chloromethane, a tetrahedral adduct is formed which is thought to be analogous to the tetrahedral intermediate formed during catalysis. This inhibitor complex has been crystallized as a dimer in space group $P4_12_12$. The structure has been refined at 2.14 Å resolution to an R value of 21.2% (free R = 25.2%). Conformational differences between δ-chymotrypsin and chymotrypsinogen in the region of the flexible autolysis loop (residues 145–150) were observed. This is the first crystal structure of δ-chymotrypsin and includes two residues which are disordered in previous crystal structures of active chymotrypsin. A difference of 11.3 Å^2 between the average B values of the monomers within the asymmetric unit is caused by lattice-disordering effects approximating to rotation of the molecules about a crystallographic screw axis. The substrate-binding mode of the inhibitor was similar to other chymotrypsin peptidyl inhibitor complexes, but this is the first published chymotrypsin structure in which the tetrahedral chloromethyl ketone transition-state analogue is observed. This structure is compared with that of a similar tetrahedral transition-state analogue which does not alkylate the active-site histidine residue.

1. Introduction

The structure and mechanism of the serine protease chymotrypsin have been investigated in detail (Matthews *et al.*, 1967; Blow *et al.*, 1969; Blow, 1976). The enzyme is composed of two β-barrels, which are thought to have evolved by gene duplication of a less active ancestral protease (McLachlan, 1979). Chymotrypsin is a digestive enzyme that hydrolyzes proteins in the small intestine and, because of its proteolytic activity, it is stored and secreted into the small intestine as the inactive precursor chymotrypsinogen. In the small intestine, chymotrypsinogen is cleaved by trypsin at the peptide bond following Arg15, yielding the fully active π-chymotrypsin. Subsequent autocatalytic hydrolysis of the bonds following residues 13, 146 and 148 and release of the resulting dipeptides gives rise to the δ, κ and α forms of the enzyme (Fig. 1). α- and

γ-chymotrypsin are covalently identical but conformationally different and exist in a pH-dependent equilibrium.

The first step in the pathway in Fig. 1 (cleavage of the Arg15–Ile16 bond) brings about complete activation of chymotrypsinogen by liberation of the α-amino group of Ile16. Translation of this liberated group by 12 Å to form a salt bridge with Asp194 provides the driving force for the formation of a productive binding site. The π and δ forms, although rapidly converted to γ- and α-chymotrypsin under conditions of high enzyme concentration and low substrate concentration, are thought to be the most abundant in the gut (Sharma & Hopkins, 1979). While the biochemical behaviour of δ- and γ-chymotrypsin is in many ways identical, some differences have been noted and explained by the presence in the δ form of a complete autolysis loop. The two forms differ strikingly in their susceptibility to inactivation at high pH, which is caused by the loss of the salt bridge between Ile16 and Asp194. It has been observed that the intact loop adjacent to the active site of δ-chymotrypsin hinders reversible inactivation at high pH, making it 80 times more active than γ-chymotrypsin at pH 11 (Valenzuela & Bender, 1969).

The mechanism of inactivation of δ-chymotrypsin also differs from that of α- and γ-chymotrypsin, which adopt a third conformation – different to those of both active chymotrypsin and chymotrypsinogen – upon inactivation (Mavridis *et al.*, 1974). It is thought that δ-chymotrypsin is restricted from adopting alternative conformations by the presence of the autolysis loop and may oscillate between active and chymotrypsinogen-like structures (Ghelis *et al.*, 1975). A final effect of the cleavage of the Tyr146–Thr147 bond is an increased interaction between δ-chymotrypsin molecules at low pH (Neet *et al.*, 1974) owing to the creation of a free carboxyl group on Tyr146.

The only crystallographic study carried out on δ-chymotrypsin to date is that of Kraut *et al.* (1970), who calculated 5 Å difference density maps of π- and δ-chymotrypsin and concluded that the overall structures of the π, δ and γ forms were similar.

The inhibitor used in this study was 2-^{13}C-enriched benzyloxycarbonylglycylglycylphenylalanyl chloromethane [Z-Gly-Gly-(2-^{13}C)Phe-CH_2Cl] (Fig. 3), a substrate-derived inhibitor which was used in ^{13}C NMR experiments to study oxyanion formation in both chymotrypsin and subtilisin (O'Connell & Malthouse, 1995). Chloromethane inhibitors alkylate $N^{\varepsilon 3}$ of the imidazole ring of the active-site histidine residue in serine proteases (Ong *et al.*, 1965). X-ray crystallographic evidence (Poulos *et al.*, 1976; James *et al.*, 1980) suggests that the active-site serine adds to the inhibitor to form a tetrahedral adduct analogous to the tetrahedral intermediate thought to be formed during catalysis (Fig. 3). ^{13}C NMR has been used to confirm that the hemiketal C atoms in these chloromethane-inhibitor complexes are sp^3 hybridized (Malthouse *et al.*, 1983, 1985; Finucane *et al.*, 1989; Finucane & Malthouse, 1992; O'Connell & Malthouse, 1995). ^{13}C NMR has also been used to determine the degree of oxyanion stabilization in these tetrahedral adducts, which has provided important insights into how the serine proteases stabilize tetrahedral intermediates during catalysis. However, it has been suggested that alkylation of the active-site histidine by chloromethane inhibitors could force the oxyanion out of its optimal position for forming hydrogen bonds in the oxyanion hole (Liang & Abeles, 1987). Therefore, one of the aims of this study was to determine whether this was true.

Because the substrate residues of these inhibitors can easily be altered, they also find use as specific protease inhibitors, many of which are pharmaceutically important (Banner &

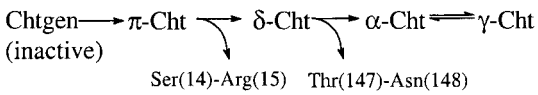

Figure 1
Activation scheme of chymotrypsinogen.

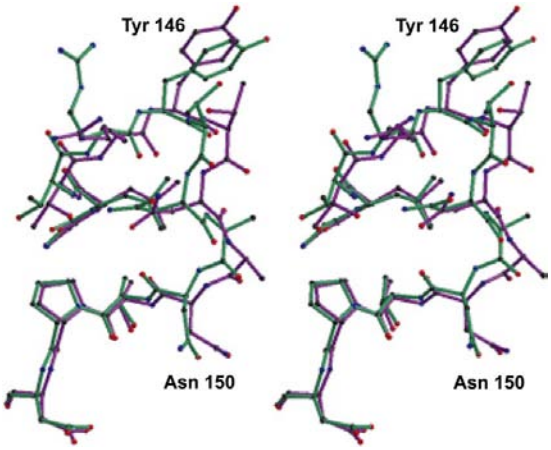

Figure 2
The autolysis loops of δ-chymotrypsin and chymotrypsinogen. The autolysis loop of δ-chymotrypsin is shown in cyan and that of chymotrypsinogen is shown in green.

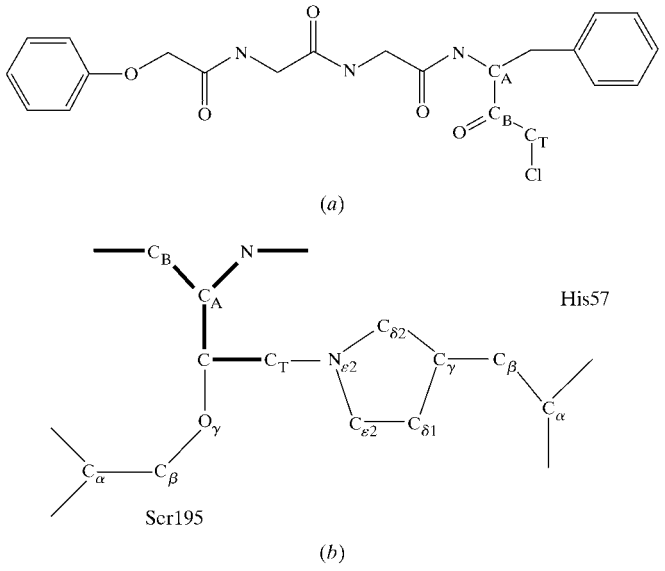

Figure 3
(*a*) The inhibitor Z-Gly-Gly-Phe-CH_2Cl; (*b*) its mode of binding to His57 and Ser195.

Hadvàry, 1991; Navia *et al.*, 1989). Crystals structures of several serine proteases with bound chloromethane inhibitors have been solved, including an unrefined 2.7 Å γ-chymotrypsin structure with incomplete inhibitor electron density (Segal *et al.*, 1971). In that structure, however, it was only possible to locate the peptidyl portion of the inhibitor (using difference maps and inhibitors of various peptide lengths) owing to non-isomorphism of the native and inhibited crystals.

Here, we describe the crystal structure of δ-chymotrypsin at 2.14 Å covalently bound to the inhibitor Z-Gly-Gly-Phe-CH_2Cl and contrast it with the structures of γ-chymotrypsin and, in the region of the autolysis loop, chymotrypsinogen. Furthermore, a marked difference between the average *B* values of the molecules within the asymmetric unit has revealed an unusual lattice effect in this crystal structure, which is described.

2. Materials and methods

2.1. Crystallization and data collection

Z-Gly-Gly-(2-^{13}C)Phe-CH_2Cl inhibited δ-chymotrypsin was prepared as previously described (O'Connell & Malthouse, 1995). Crystals were grown using the hanging-drop vapour-diffusion method at 298 K using 30 mg ml^{-1} protein equilibrated against 2.6 *M* ammonium sulfate, 10 m*M* $CoCl_2$ and 200 m*M* MES–HCl at pH 6.5. Crystals grew as large tetragonal bipyramids in space group $P4_12_12$, with unit-cell parameters $a = b = 121.4$, $c = 116.1$ Å. X-ray diffraction data were collected on a 300 mm MAR Research imaging-plate scanner at 293 K to a resolution of 2.14 Å using synchrotron radiation from the EMBL beamline X11 at the DORIS storage ring, DESY, Hamburg (data-collection and processing statistics are listed in Table 1).

2.2. Structure solution and refinement

The structure was determined by molecular replacement using the *CCP*4 (Collaborative Computational Project, Number 4, 1994) version of the program *AMoRe* and the γ-chymotrypsin coordinate set of Brady *et al.* (1990) as a search model. The inhibitor was built using HyperChem (Hypercube Inc., 1115 NW 4th Street, Gainesville, FL 32601, USA) and was geometry-optimized before being fitted to difference electron density. The covalent bond lengths from C_T of the inhibitor to His57 $N^{\varepsilon 2}$ and from C of the inhibitor to Ser195 O^{γ} were restrained in *PROTIN* to 1.45 and 1.47 Å, respectively. The structure of chymotrypsinogen (Hecht *et al.*, 1991) was used as a guide in fitting the autolysis loop of δ-chymotrypsin. Maximum-likelihood refinement was carried out with twofold non-crystallographic symmetry (NCS) restraints using the program *REFMAC* (Murshudov *et al.*, 1997) and ordered water molecules were added using the program *ARP* (Lamzin & Wilson, 1997). After initial refinement, a chloride ion was located and double occupancy was observed for several residues. The final model consisted of a dimer containing 3528 protein atoms, 58 inhibitor atoms, one chloride ion and 381 water molecules. An alternative conformation was added for Met192 of molecule *A*. 89.6% of residues fell within the favoured regions and 10.4% within the allowed regions of the Ramachandran plot (Ramachandran & Sasisekharan, 1968). A summary of the refinement statistics is given in Table 1.

3. Results and discussion

3.1. Description of the structure

The overall structure of δ-chymotrypsin was identical to that of γ-chymotrypsin, except in the region of the autolysis loop (residues 145–150) which is intact only in the δ form. Residues Ser11 and Gly12 are ordered in both molecules and Leu13 is ordered in molecule *B*, making δ-chymotrypsin the only active form of the enzyme in which all residues are located [residues 11–13 are missing from the structures of the α and γ forms in the Protein Data Bank (PDB; Bernstein *et al.*, 1977)]. These residues point toward the solvent in δ-chymotrypsin and are held in position by crystal contacts. Leu13 of molecule *B* is additionally stabilized by an interaction with Leu143 O *via* an ordered water molecule. The side chains of the following residues are disordered (or partially disordered) and are excluded from the model: Gln7 and lysines 36, 79, 84, 87 and 170 of molecule *A*; Lys36, Lys79 and Arg145 of molecule *B*.

A single chloride ion was located close to the crystallographic twofold NCS axis. The chloride binds to residues 59 and 90 of molecules *A* and *B*, respectively, and is surrounded by four ordered water molecules. This chloride ion is absent from previous chymotrypsin structures and binds at a different location to the sulfate ion which has been observed in several crystal structures of γ-chymotrypsin. No cobalt was present, despite the fact that crystals failed to grow when $CoCl_2$ in the reservoir solution was replaced with other chloride salts.

The *B* factors were considerably higher in molecule *A* than in molecule *B* (35.2 *versus* 23.9 Å^2) of the asymmetric unit. Molecules *A* and *B* were least-squares fitted and all regions of

Table 1
Data collection and refinement statistics.

Figures in parentheses refer to the highest resolution shell (2.18–2.14 Å).

Total observations	308959
Unique reflections	48065
$R_{\rm merge}$† (%)	8.1 (43.5)
Completeness (40–2.14 Å) (%)	99.6 (100)
I/σ_I	22.6 (4.3)
Resolution range (Å)	40.0–2.14
No. of reflections used	48013 (2370)
No. of protein atoms in asymmetric unit	3528
No. of ligand atoms in asymmetric unit	58
R factor‡ (%)	21.2
Free *R* factor§ (%)	25.1
R.m.s.d. of bond lengths (Å)	0.018
R.m.s.d. of bond angles (°)	1.9

† $R_{\rm merge} = 100\sum_h[\sum_i |I_{i(h)} - \langle I_{(h)}\rangle|]\sum_i I_{(h)}$. ‡ *R* factor $= \sum||F_o| - |F_c||/\sum|F_o|$. § $R_{\rm free}$ is the *R* factor calculated using 10% of the data that were excluded from refinement.

Table 2
R.m.s. deviation of the autolysis loop of δ-chymotrypsin from that of chymotrypsinogen, calculated using *DIFRES* (Collaborative Computational Project, Number 4, 1994).

A side-chain deviation of zero indicates that the residues are identical in orientation, not position.

	R.m.s. deviation (Å^2)	
Residue	Main chain	Side chain
142	0.5	0.0
143	0.8	0.8
144	0.8	2.4
145	1.2	3.7
146	1.0	2.2
147	2.0	2.8
148	2.0	2.1
149	1.9	3.5
150	1.0	0.0
151	0.6	0.5

significant deviation were found to be on surface loops involved in intermolecular contacts. The regions of highest *B* factor were residues 10–12 of molecule *A*, which are poorly ordered, and residues 74–78 of molecule *A*, which appeared to occupy two conformations but could not be clearly distinguished at this resolution. The side chain of Met192 of molecule *A* occupied two conformations, one along the protein surface and one pointing towards the solvent. The conformer pointing towards the solvent is stabilized by the shielding effect of the peptide chain of the bound inhibitor and by the benzyloxycarbonyl group of the NCS-related inhibitor which is bound to molecule *B*. No conformer pointing towards the solvent was observed for this residue in molecule *B*, which is less shielded from the solvent. The r.m.s. deviations between main-chain and side-chain atoms for the two molecules in the asymmetric unit are 0.28 and 0.79 Å, respectively, after refinement with weak NCS restraints (weak main chain and side chain as specified in *PROTIN*).

The inhibitor (Fig. 3) binds in an antiparallel β structure similar to previous structures (Segal *et al.*, 1971), except that there appears to be no hydrogen bond between the carbonyl O atom of Gly216 and atom N3 of the inhibitor. This is probably because of steric repulsion between the phenyl group of the inhibitor and the large side chain of Trp172. The benzyloxycarbonyl portion was well ordered, despite the lack of hydrogen bonding to the protein in this region. This can be seen in Fig. 4, which shows the covalently bound inhibitor and an $F_o - F_c$ electron-density map at the active site, which was calculated using the phases of the refined model with the inhibitor omitted. The previously unobserved distortions of residues His57 and Ser195 of the active site were significant, with shifts of 0.7 and 1.0 Å for atoms His57 $N^{\varepsilon 2}$ and Ser195 O, respectively. This decreases the distance between these two atoms from 3.8 Å in uninhibited γ-chymotrypsin to 3.0 Å in this structure. The inhibitors of molecules *A* and *B* in the asymmetric unit lie within 5 Å of each other and have very similar geometry. The inhibitor binding and geometry are detailed in Table 3.

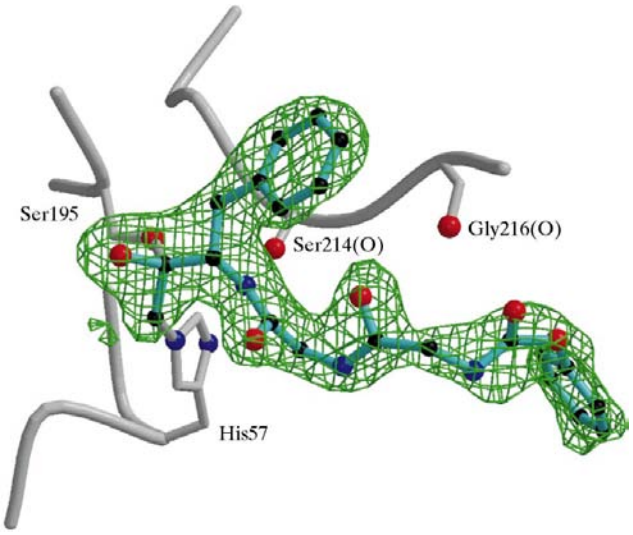

Figure 4
$F_o - F_c$ electron density contoured at the 2.5σ level at the catalytic site. The map was calculated using phases from the model refined prior to inclusion of the inhibitor. The covalent bonds between the inhibitor and residues Ser195 and His57 are shown.

Table 3
Bonding of Z-Gly-Gly-Phe-CH_2Cl inhibitor to δ-chymotrypsin.

The approximately tetrahedral geometry around atom C of the inhibitor is shown.

Atoms	Angle (°)
Ser195 O_G–CMK C–CMK O	95
Ser195 O_G–CMK C–CMK C_A	117
Ser195 O_G–CMK C–CMK C_T	101
CMK C_A–CMK C–CMK C_T	119
CMK O–CMK C–CMK C_A	121
CMK C–CMK C_A–CMK C_B	99
CMK C–CMK C_A–CMK N	110

Main-chain interactions of the inhibitor peptide chain with the substrate-binding pocket of δ-chymotrypsin.

Bonded atoms	Distance (Å)
A193 N–CMK O1	3.0
A214 O–CMK N1	2.7
A216 N–CMK O3	3.2

3.2. Comparison of structures

Our refined model of δ-chymotrypsin inhibited by Z-Gly-Gly-(2-^{13}C)Phe-CH_2Cl was compared with the structure, determined by Brady *et al.* (1990), of the adduct formed between α-chymotrypsin and *N*-acetyl-L-leucyl-L-phenylalanyl trifluoromethyl ketone. Owing to the alkylation of His57 $N^{\varepsilon 2}$ in the chloromethane-inhibitor adduct, the hemiketal C atom of the inhibitor is only 2.72 Å from His57 $N^{\varepsilon 2}$ (Fig. 5*a*). This distance is 4.12 Å in the trifluoromethyl ketone inhibitor adduct (Fig. 5*b*), in which the histidine is not alkylated. Therefore, alkylation of His57 increases the distance between His57 $N^{\delta 1}$ and the carboxylate C atom of Asp102 by 0.44 Å (Fig. 5). It also only increases the hydrogen bonds from the oxyanion to the backbone NH groups of Gly193 and Ser195 by 0.18 and 0.65 Å, respectively (Fig. 5). Thus, while alkylation of the active-site histidine residue causes some movement of the active-site groups, the tetrahedral adduct formed with chloromethane inhibitors are expected to be reasonable

analogues of tetrahedral intermediates formed during catalysis.

The refined model of δ-chymotrypsin was also compared (Fig. 6) with the structure of chymotrypsinogen (Hecht *et al.*, 1991) by least-squares fitting of the main-chain atoms (excluding residues 10–16) using the program *LSQKAB* (Kabsch, 1978). The overall structures were found to be similar, with r.m.s. deviations of 0.4 and 1.25 Å for main-chain and side-chain atoms, respectively, except in the region of Ile16 and the autolysis loop (Fig. 2; Table 2). The movement of Ile16 to form a salt bridge with Asp194 upon activation has been extensively studied (Freer *et al.*, 1970) and its position in δ-chymotrypsin is identical to that in other active forms.

The autolysis loop is known from chymotrypsinogen structures to be inherently flexible and has different conformations in two chymotrypsinogen structures in the PDB. All comparisons were made with the autolysis loop of the BPTI-bound chymotrypsinogen structure of Hecht *et al.* (1991), which resembles that of δ-chymotrypsin more closely than that of Wang *et al.* (1985). The differences include a rotation of ∼150° of the carbonyl bond of Asn148 and a slight movement of the loop towards the centre of the protein. Two notable differences between the structures of chymotrypsinogen and δ-chymotrypsin may contribute to relocation of the loop. Firstly, the movement of residues Ile16–Gly19 upon activation of chymotrypsinogen causes the loss of the hydrogen bond between Asn18 and Thr144. Secondly, the carbonyl O atom of Ile16 of δ-chymotrypsin lies close to the carbonyl O atom of residue Leu143 (3.4 Å; 3.0 Å from Ile16 of δ-chymotrypsin to Leu143 of the superimposed chymotrypsinogen structure). The autolysis loop is involved in crystal contacts in chymotrypsinogen and α-, π- and δ-chymotrypsin and it is evident that the change in conformation was also a consequence of differences in crystal packing (Table 4). The terminal atoms of the side chains of Arg145 and Tyr146 of δ-chymotrypsin and chymotrypsinogen deviate by 4.0 Å to form hydrogen bonds with symmetry-related molecules. A large shift in the position of Ser76 is caused solely by intermolecular contacts and an examination of other chymotrypsin structures revealed a range of positions for this residue.

As well as providing a more complete structure of active chymotrypsin, this structure allows a more detailed examination of this intermediate form of chymotrypsin and its covalent interactions with chloromethane inhibitors. Determination of a subtilisin-bound chloromethane crystal structure will permit an interesting comparison of the modes of stabilization of the tetrahedral intermediate in these enzymes.

Table 4
Intermolecular contacts (≤3.6 Å) in δ-chymotrypsin and chymotrypsinogen.

δ-chymotrypsin

	Distance (Å)
Tyr146 O–Lys175 NZ	2.6
Arg148 O–Lys175 NZ	3.6

Chymotrypsinogen

	Distance (Å)
Arg145 NH1–Tyr171 OH	3.1
Arg145 NH1–Ala185 O	3.5
Arg145 NH1–Ser223 O	3.0
Tyr146 OH–Lys170 O	3.5

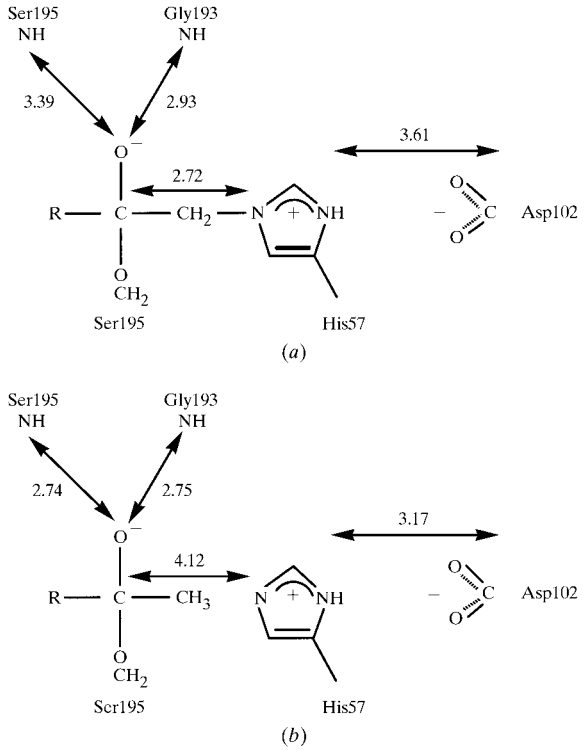

Figure 5
A comparison of the structures of the tetrahedral adducts formed when chymotrypsin is inhibited by (*a*) Z-Gly-Gly-(2-^{13}C)Phe-CH_2Cl and (*b*) Z-Leu-Phe-CF_3.

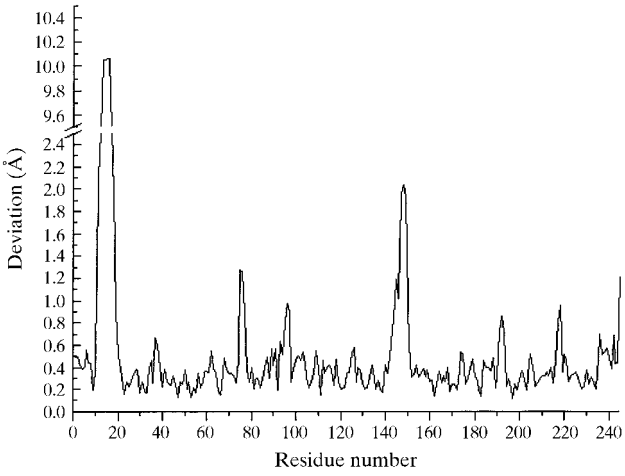

Figure 6
Plot of main-chain and side-chain differences between δ-chymotrypsin and chymotrypsinogen.

3.3. Extended lattice disorder in δ-chymotrypsin

A marked difference between the average *B* values of the molecules within the asymmetric unit pointed towards an unusual lattice effect in this crystal structure. Normally, the observed effect of lattice interactions is the localized immobilization of side chains or surface loops, as exemplified by the correlation of residue *B* values with the fractional accessible surface of that residue in a given crystal lattice. In some cases, it is possible to observe a second, long-range lattice effect owing to static or dynamic rotational disorder about a crystallographic screw axis. This type of disorder is revealed by a correlation between *B* value and distance from the crystallographic axis. Lattice interactions were investigated by plotting the difference in *B* factor of each residue (ΔB) between molecules *A* and *B* of the asymmetric unit against the difference in their distance from the screw axis (ΔR; Fig. 7). Despite scattering of the points caused by non-equivalent local lattice effects, a correlation between ΔB and ΔR can be clearly observed (correlation 0.44, or 0.48 when residues 10–12 and 73–76 are excluded based on their large non-equivalent local lattice effects). This effect was first noticed in the case of cytochrome *c*′ (Finzel & Salemme, 1985) and little has been published on the subject since. The plot indicates an increase of 18 Å^2 owing to long-range disorder at the periphery of molecule *A*, suggesting an axial rotation about the screw axis of approximately 0.5° that produces a maximum displacement of 0.8 Å. The slightly higher than average *R* value of the refined structure is probably a consequence of this extended lattice disorder. Lattice interactions of this type can equally arise in cases where only a single molecule occupies the asymmetric unit and could easily be mistaken for increased inherent mobility resulting from secondary-structure elements within the protein. This highlights the need to closely inspect the crystal packing before invoking *B* factors as indicators of protein-domain mobility.

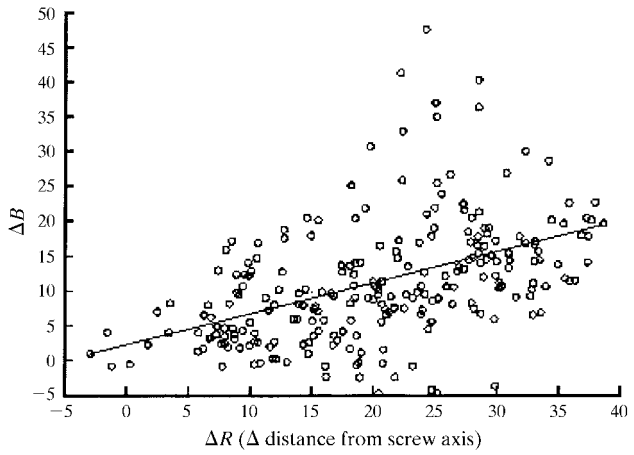

Figure 7
Plot of the difference in mean backbone *B* value (ΔB) between corresponding residues of δ-chymotrypsin monomers against their difference in radial distance (ΔR) from the crystal screw axis on which the *B* molecules are aligned. The least-squares line suggests that the long-range disorder contributes up to 18 Å^2 to the residues furthest from the screw axis. Large deviations from the least-squares line correspond to non-equivalent crystal contacts.

AMS was supported by a Forbairt fellowship. MAW was supported by an EC Institutional Fellowship, contract CT 930485.

References

Banner, D. W. & Hadvàry, P. (1991). *J. Biol. Chem.* **266**(30), 20085–20093.
Bernstein, F. C., Koetzle, T. F., Williams, G. J. B., Meyer, E. F. Jr, Brice, M. D., Rodgers, J. R., Kennard, O., Shimanouchi, T. & Tasumi, M. (1977). *J. Mol. Biol.* **112**, 535–542.
Blow, D. M. (1976). *Acc. Chem. Res.* **9**, 145–152.
Blow, D. M., Birktoft, J. J. & Hartley, B. S. (1969). *Nature (London)*, **21**, 337–340.
Brady, K., Wei, A., Ringe, D. & Abeles, R. H. (1990). *Biochemistry*, **29**, 7600–7607.
Collaborative Computational Project, Number 4 (1994). *Acta Cryst.* D**50**, 760–763.
Finucane, M. D., Hudson, E. A. & Malthouse, J. P. G. (1989). *Biochem. J.* **258**, 853–859.
Finucane, M. D. & Malthouse, J. P. G. (1992). *Biochem. J.* **286**, 889–900.
Finzel, B. C. & Salemme, F. R. (1985). *Nature (London)*, **315**, 686–688.
Freer, S. T., Kraut, J., Robertus, J. D., Wright, H. T. & Xuong, N. H. (1970). *Biochemistry*, **9**, 1997–2009.
Ghelis, C., Labouesse, J. & Labouesse, B. (1975). *Eur. J. Biochem.* **59**, 159–166.
Hecht, H. J., Szardenings, M., Collins, J. & Schomburg, D. (1991). *J. Mol. Biol.* **220**(3), 711–722.
James, M. N. G., Brayer, G. D., Delbaere, L. T. J., Sielecki, A. R. & Gertler, A. (1980). *J. Mol. Biol.* **139**, 423–438.
Kabsch, W. (1978). *Acta Cryst.* A**32**, 922–923.
Kraut, J., Wright, H. T., Kellerman, M. & Freer, S. T. (1970). *Biochemistry*, **58**, 304–311.
Lamzin, V. S. & Wilson, K. S. (1997). *Methods Enzymol.* **277**, 269–305.
Liang, T. C. & Abeles, R. H. (1987). *Biochemistry*, **26**, 7603–7608.
McLachlan, A. D. (1979). *J. Mol. Biol.* **128**(1), 49–79.
Malthouse, J. P. G., Mackenzie, N. E., Boyd, A. S. F. & Scott, A. I. (1983). *J. Am. Chem. Soc.* **105**, 1685–1686.
Malthouse, J. P. G., Primrose, W. U., Mackenzie, N. E. & Scott, A. I. (1985). *Biochemistry*, **24**, 3478–3487.
Matthews, B. W., Sigler, P. B., Henderson, R. & Blow, D. M. (1967). *Nature (London)*, **214**, 652–656.
Mavridis, A., Tulinsky, A. & Liebman, M. N. (1974). *Biochemistry*, **13**(18), 3661–3666.
Murshudov, G. N., Vagin, A. A. & Dodson, E. J. (1997). *Acta Cryst.* D**53**, 240–255.
Navia, M. A., Fitzgerald, P. M., McKeever, B. M., Leu, C. T., Heimbach, J. C., Herber, W. K., Sigal, I. S., Darke, P. L. & Springer, J. P. (1989). *Proc. Natl Acad. Sci. USA*, **86**, 7–11.
Neet, K. E., Sackrison, K. M., Ainslie, G. R. & Barritt, L. C. (1974). *Arch. Biochem. Biophys.* **160**, 569–576.
O'Connell, T. P. & Malthouse, J. P. G. (1995). *Biochem. J.* **307**, 353–359.
Ong, E. B., Shaw, E. & Schoellmann, G. (1965). *J. Biol. Chem.* **240**, 694–698.
Poulos, T. L., Alden, R. A., Freer, S. T., Birktoft, J. J. & Kraut, J. (1976). *J. Biol. Chem.* **251**, 1097–1103.
Ramachandran, G. N. & Sasisekharan, V. (1968). *Adv. Protein Chem.* **23**, 283–437.

Segal, D. M., Powers, J. C., Cohen, G. H., Davies, D. R. & Wilcox, P. E. (1971). *Biochemistry*, **10**(20), 3728–3737.
Sharma, S. T. & Hopkins, T. R. (1979). *Biochemistry*, **18**(6), 1008–1013.
Valenzuela, P. & Bender, M. L. (1969). *Proc. Natl Acad. Sci. USA*, **63**, 1214–1221.
Wang, D., Bode, W. & Huber, R. (1985). *J. Mol. Biol.* **185**(3), 595–624.